MADRID
inter.noise 2019
June 16 - 19
NOISE CONTROL FOR A BETTER ENVIRONMENT

A preliminary study of the acoustic attenuation of a thin acoustic liner

Yang, Cheng[1]
Zhang, Penglin[2]
Zhong, Tingsheng[3]
Institute of Vibration Shock and Noise, School of Mechanical Engineering, Shanghai Jiao Tong University
No. 800 Dongchuan Road, Shanghai, China

ABSTRACT

This paper presents a preliminary study of a thin acoustic liner for duct noise control applications. Conventional resonant type acoustic liners are usually less effective for low-frequency noise reduction unless a thick backing air cavity is used. To overcome this problem, a microperforated panel with each hole being axially extruded to form an extended tube is used to replace the covering panel. By doing so, the resonance frequency of the liner can be significantly reduced, as compared with the conventional liner of the same thickness. To characterize its acoustic property, a theoretical model is developed by using the transfer matrix method to obtain the surface impedance of the liner. An impedance tube test is then made to examine the accuracy of the model. The proposed model is then used to design an acoustic liner which is tested in a flow duct.

Keywords: Microperforated panel, duct noise, acoustic liner
I-INCE Classification of Subject Number: 37

1. INTRODUCTION

A resonant type acoustic liner often consists of a perforated/microperforated panel on top of a backing air cavity [1, 2]. Due to the quarter wavelength rule inherent such a system, a thicker liner has to be used in order to achieve effective acoustic absorption at low frequencies, which becomes a challenge to the deployment of noise control technique in compact systems.

A variety of efforts has been made to improve the low frequency acoustic absorption while maintaining or reducing the liner thickness in the meantime. Tao [3] considered the use of a close-box loudspeaker with a shunted circuit to replace the rigid backing wall of a conventional liner, leading to a compact solution to low frequency absorption problem where a deep backing cavity is required. Chen [4] designed a coiled-up air channel at the

[1] cheng.yang@sjtu.edu.cn
[2] aaronzpl@sjtu.edu.cn
[3] zhongtingsheng@sjtu.edu.cn

measured result show that the wavelength, at which the maximum absorption is achieved, to the liner thickness yields a value of 38.5. Sugimoto [5] proposed a folded liner containing an L-shaped backing cavity geometry. The design allows the liner to be fitted in a shallower space in the aircraft engine nacelle to meet the mechanical design constraint. Gai [6] integrated a membrane attached with mass blocks into the MPP panel. The additional resonance introduced by the structural vibration results in an increase in absorption at low frequencies.

This work is concerned with improving the low frequency absorption of an acoustic liner by using the extended tube technique which was proposed by Lu in 2001 [7]. An extended tube is one which grow axially from the hole in a standard perforated panel. By increasing the length of the narrow tube, a considerable increase in energy loss occurs in the shear layer above the tube wall so that low frequency absorption can be improved. Although the low frequency performance is improved, the increased energy dissipation mechanism will also result in an increase of the resistance at higher frequencies where an impedance mismatch might occur, giving rise to a poor acoustic absorption. To achieve a broadband absorption effect, Chang [8] used an array of extended tubes with different lengths. Later, Huang [9] developed an analytical model to predict the acoustic property of such type of liner. The aforementioned work, however, often examines the liner performance through the impedance tube measurement. It has already been shown that the acoustic absorption coefficient measured in an impedance tube may not always indicate the *in situ* noise control performance in a compact system [10]. Probably the first work to investigate effect of an extended tube liner in a confined space was made by Simon [11] where the liner was tested in a flow duct test rig. However, due to confidential reasons, little results are provided.

In this work, a preliminary study of the extended tube liner which could be an alternative to conventional liner is made. An analytical model is developed to predict the surface impedance of the liner for the normal incidence case and the model is then examined by comparing with existing models in the literature. An impedance tube test is also made to further examine the accuracy of the proposed mode. Then, a prototype is made by the additive manufacturing technique and is tested in a flow duct test rig.

2. MODEL DEVELOPMENT

2.1 Acoustics of an extended tube

An extended tube liner is shown schematically in Fig. 1. The tubes are assumed to have negligible wall thickness and have identical length l_t. The perforation of the microperforated panel is σ. An air cushion with a depth of $h+ l_t$ is placed between the panel and the rigid backing wall. For simplicity of the model development, the liner is assumed to be laterally periodic so that the problem becomes two-dimensional.

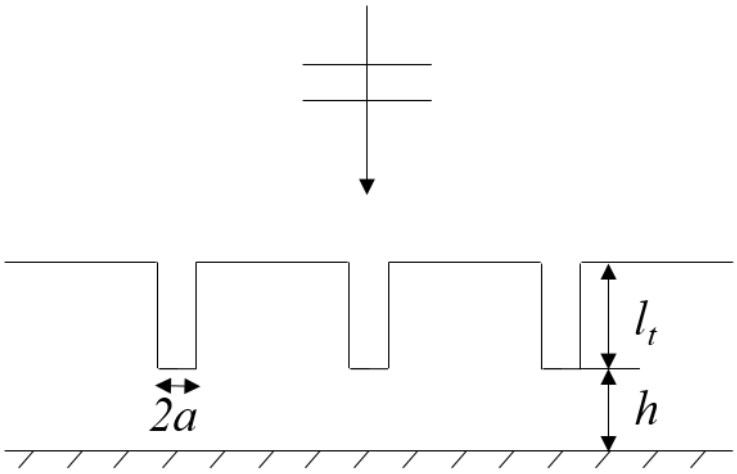

Fig.1 Schematics of an extended tube liner.

Assuming small acoustic perturbations and neglecting the higher order terms, the density ρ, particle velocity v, pressure p and temperature T are governed by:

$$\frac{\partial \rho}{\partial t} + \rho_0 \frac{\partial v}{\partial x} = 0 \tag{1}$$

$$\rho_0 \frac{\partial v}{\partial t} = -\frac{\partial p}{\partial x} + \frac{\mu}{r}\frac{\partial}{\partial r}\left(r\frac{\partial v}{\partial r}\right) \tag{2}$$

$$\rho_0 c_p \frac{\partial T}{\partial t} - \frac{\partial p}{\partial t} = \frac{k}{r}\frac{\partial\left(r\frac{\partial T}{\partial r}\right)}{\partial r} \tag{3}$$

$$\frac{p}{p_0} = \frac{\rho}{\rho_0} + \frac{T}{T_0} \tag{4}$$

where μ, k and c_p, and are fluid viscosity, heat transfer coefficient and specific heat, respectively, and the subscript *0* indicates ambient-field variables. Here, it is assumed that the tube walls are acoustically rigid, so $v(a) = 0$.

Assuming harmonic solutions

$$\begin{aligned} p &= P(r)e^{j\omega t - jqx}, \qquad v = V(r)e^{j\omega t - jqx} \\ \rho &= R(r)e^{j\omega t - jqx}, \qquad T = T(r)e^{j\omega t - jqx}. \end{aligned} \tag{5}$$

the governing equations Equations 1-4 can be rearranged as

$$j\omega R - jq\rho_0 V = 0 \tag{6}$$

$$\frac{d^2V}{dr^2} + \frac{1}{r}\frac{dV}{dr} - \frac{j\omega\rho_0}{\mu}V = -\frac{jq}{\mu}P \tag{7}$$

$$\frac{d^2T}{dr^2} + \frac{1}{r}\frac{dT}{dr} - \frac{j\omega\rho_0 c_p}{k}T = -\frac{j\omega}{k}P \tag{8}$$

$$\frac{P}{p_0} = \frac{R}{\rho_0} + \frac{T}{T_0} \tag{9}$$

For frequencies where the acoustic wavelength is much larger than the hole radius, the radial variation of the acoustic pressure can be neglected, therefore, $P(r) = P_0$ and

$$V(r) = -\frac{jqP_0}{\mu K_\mu^2}\left[1 - \frac{\mathrm{J}_0\left(K_\mu r\right)}{\mathrm{J}_0\left(K_\mu a\right)}\right] \tag{11}$$

where

$$K_\mu = \sqrt{-\frac{j\omega\rho_0}{\mu}} \tag{12}$$

For isothermal tube walls, T(a) = 0, thus

$$T(r) = -\frac{j\omega P_0}{kK_k^2}\left[1 - \frac{J_0(K_k r)}{J_0(K_k a)}\right] \tag{13}$$

where

$$K_k = \sqrt{-\frac{j\omega\rho_0 c_p}{k}} \tag{14}$$

By averaging the field variables over the cross section area, one obtains

$$\bar{V} = \frac{1}{\pi a^2}\int_0^a 2\pi r V(r)dr = \frac{qP_0}{\rho_0\omega}[1 - \frac{2J_1(K_\mu a)}{K_\mu a J_0(K_\mu a)}], \tag{15}$$

$$\bar{T} = \frac{1}{\pi a^2}\int_0^a 2\pi r T(r)\mathrm{d}r = \frac{P_0}{\rho_0 c_p}[1 - \frac{2\mathrm{J}_1(K_k a)}{K_k a \mathrm{J}_0(K_k a)}], \tag{16}$$

$$\bar{R} = \frac{1}{\pi a^2}\int_0^a 2\pi r R(r)\mathrm{d}r = \frac{q^2 P_0}{\omega^2}[1 - \frac{2J_1(K_\mu a)}{K_\mu a J_0(K_\mu a)}]. \tag{17}$$

By substituting Equation 16 and Equation 17 into Equation 9, along with $c^2=\gamma p_0/\rho_0$, the propagation constant can be expressed as

$$q = \pm\left(\frac{\omega}{c}\right)\sqrt{\frac{\gamma - (\gamma-1)B}{A}} \tag{18}$$

where

$$A = 1 - \frac{2\mathrm{J}_1(K_\mu a)}{K_\mu a \mathrm{J}_0(K_\mu a)}, B = 1 - \frac{2\mathrm{J}_1(K_k a)}{K_k a \mathrm{J}_0(K_k a)} \tag{19}$$

The above derivation allows the acoustic pressure and velocity between the two ends of the tube to be related in a matrix form

$$\begin{bmatrix} p_1 \\ v_1 \end{bmatrix} = \begin{bmatrix} \cos(ql_t) & \frac{j\rho_0\omega}{qA}\sin(ql_t) \\ \frac{jqA}{\rho_0\omega}\sin(ql_t) & \sin(ql_t) \end{bmatrix}\begin{bmatrix} p_2 \\ v_2 \end{bmatrix} = T_{tube}\begin{bmatrix} p_2 \\ v_2 \end{bmatrix} \tag{20}$$

2.2 Surface impedance

Upon obtaining the relation between the two ends of the tube, the surface impedance of the liner can be obtained by the transfer matrix method. The acoustic pressure at the media immediately above the panel and those at the tope of the tube follow the relation

$$\begin{bmatrix} p_0 \\ v_0 \end{bmatrix} = \begin{bmatrix} 1 & 0 \\ 0 & \sigma \end{bmatrix}\begin{bmatrix} p_1 \\ v_1 \end{bmatrix} = T_{\mathrm{air/tube}}\begin{bmatrix} p_1 \\ v_1 \end{bmatrix}, \tag{21}$$

At the bottom end of the tube, the relation reads

$$\begin{bmatrix} p_2 \\ v_2 \end{bmatrix} = \begin{bmatrix} 1 & 0 \\ 0 & 1/\sigma \end{bmatrix}\begin{bmatrix} p_3 \\ v_3 \end{bmatrix} = T_{\mathrm{tube/cavity}}\begin{bmatrix} p_3 \\ v_3 \end{bmatrix}, \tag{22}$$

By assuming an equivalent thick microperforated panel (thickness l_t), the transfer matrix for the rigid-walled backing air cavity is

$$\begin{bmatrix} p_3 \\ v_3 \end{bmatrix} = \begin{bmatrix} \cos(k_0 h) & j\rho_0 c\sin(k_0 h) \\ j\frac{\sin(k_0 h)}{\rho_0 c} & \cos(k_0 h) \end{bmatrix}\begin{bmatrix} p_4 \\ v_4 \end{bmatrix} = T_{\mathrm{cavity}}\begin{bmatrix} p_4 \\ 0 \end{bmatrix}, \tag{23}$$

Combining Equations 20-23, one obtains the transfer matrix as

$$T = T_{\text{air/tube}} T_{\text{tube}} T_{\text{tube/cavity}} T_{\text{cavity}} \begin{bmatrix} T_{11} & T_{12} \\ T_{21} & T_{22} \end{bmatrix} \tag{24}$$

where the surface impedance reads

$$Z_s = \frac{p_0 T_{11}}{v_0 T_{21}}. \tag{25}$$

3. NORMAL PLANE WAVE INCIDENCE

The proposed model is examined by comparing with the model in the literature [11]. Figure 2 shows the acoustic absorption coefficient curve for an extended tube liner with the parameters h = 20mm, r = 0.6mm and σ = 3.7%. It can be seen that the proposed model is in good agreement with that in the literature. Also shown in the figure is the one neglecting the heat transfer effect, i.e. k = 0. The curves for the two cases are hardly to be distinguished, implying that the thermal effect is not an important factor in determining the acoustic property of the liner. A calculation is also made by using the Finite Element Method (FEM) where the viscothermal effect within the extended tube is taken into account. The result shows a shift in absorption peak in the frequency spectrum. The real and imaginary part of the surface impedance is shown in Fig. 3(a) and (b), the resistance predicted by Simon [11] is greater than the proposed model but is smaller than that of the FEM result. The reactance predicted by all models collapse at low frequencies but the FEM results grows faster with frequency.

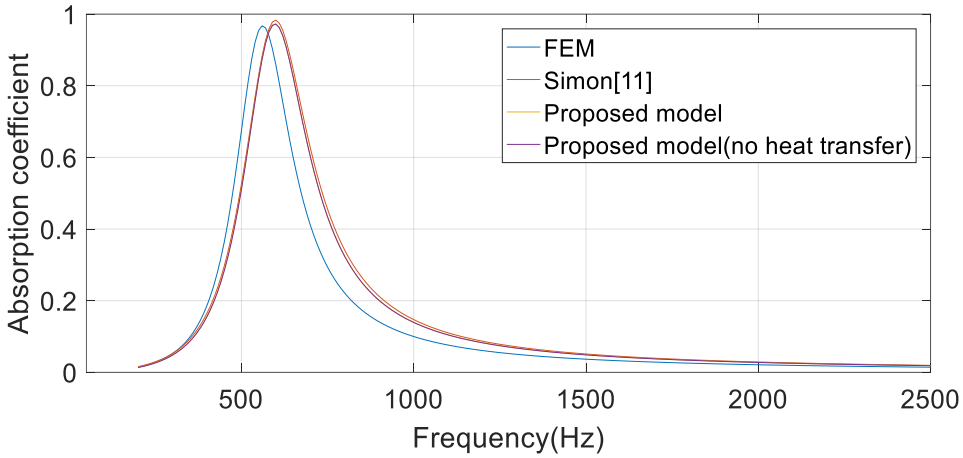

Fig. 2 Simulated acoustic absorption coefficient curves.

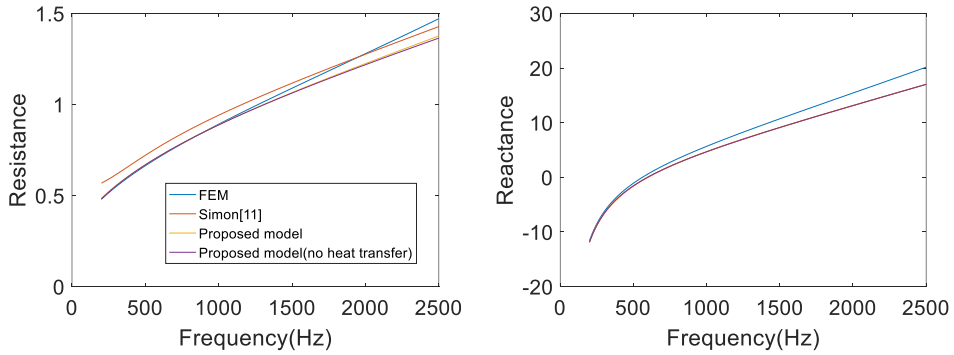

Fig. 3 Simulated surface acoustic impedance. Left: resistance; Right: reactance.

A prototype of the liner is 3D printed and is tested using the impedance tube. Parameters of the liner are: l_t = 5mm, h = 15mm and σ = 1.42%. The result is shown in

Fig. 4. It is observed that, although the proposed model is in good agreement with that in the literature, a considerable discrepancy with the measured result is found in terms of both the peak frequency and absorption coefficient value. When the prototype is installed in the impedance tube holder, tubes at the boundary are not backed by entire backing cells. A FEM model is developed to take this effect into account and the result is shown in Fig. 4. In this case, the absorption coefficient curve shows two closely spaced peaks which correspond to Helmholtz resonances associated with different cell volumes (Fig. 5). A plausible reason for the discrepancy between the proposed model and the measurement result is the end correction for the extended tube. Further work should be made on this to improve the prediction result.

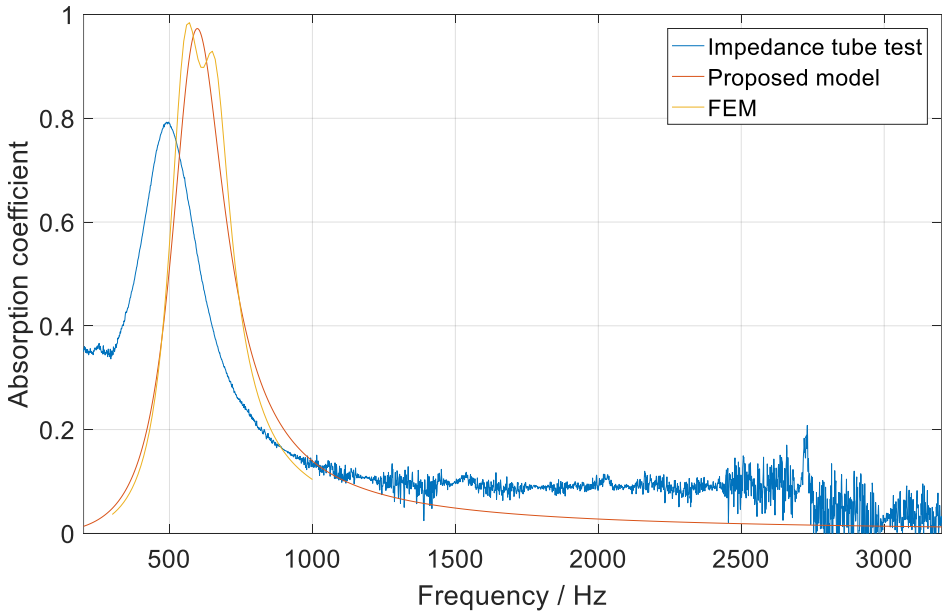

Fig. 4 Simulated and measured acoustic absorption coefficient curves.

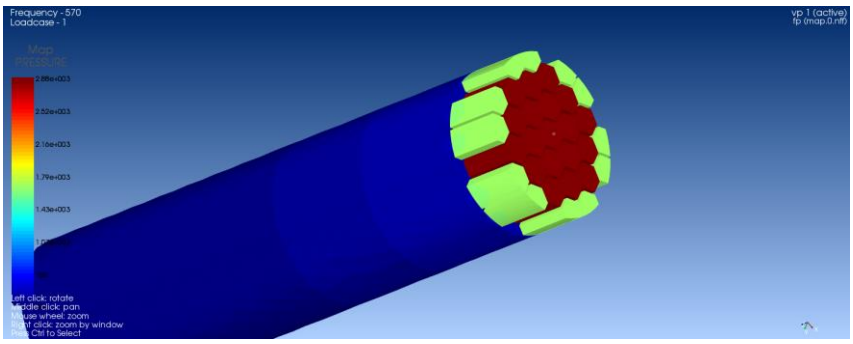

(a)

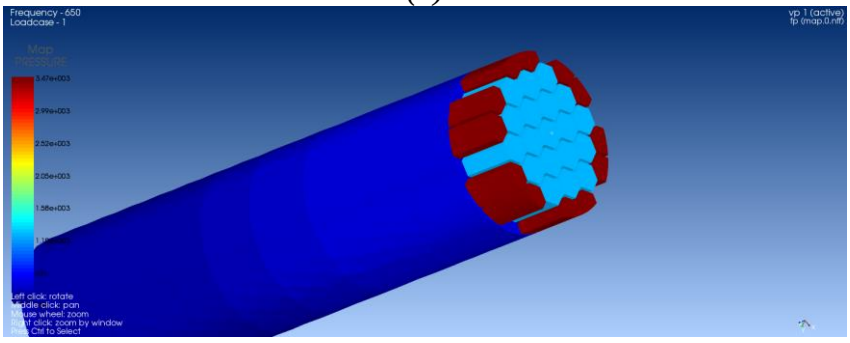

(b)

Fig. 5 Acoustic pressure distribution in the backing cells at different peak frequencies. (a) 570Hz; (b) 650Hz;

4. FLOW DUCT TEST

4.1 Description of the test rig

The noise control performance of the extended tube liner is examined on the flow duct in the State Key Laboratory of Mechanical System and Vibration at Shanghai Jiao Tong University. A photo of the flow duct is shown in Fig. 6. The air flow is injected by a centrifugal fan into the ducted system. The background noise generated by the fan is reduced by the silencer downstream of the fan and further reduced by a liner installed immediately downstream of the contraction. The facility enables a maximum mean flow speed of 0.22Mach. A plane wave acoustic source is generated by a loudspeaker mounted upstream of the liner section. The sound pressure level of the incidence wave is maintained at 130dB.

The 3D printed nylon liner is shown in Fig. 7 which has the dimension of 520mm*100mm*21mm. Other parameters are the same as that used in the impedance tube test. According to the proposed model, the liner is expected to achieve maximum acoustic absorption at 600Hz.

Fig. 6 Flow duct test rig.

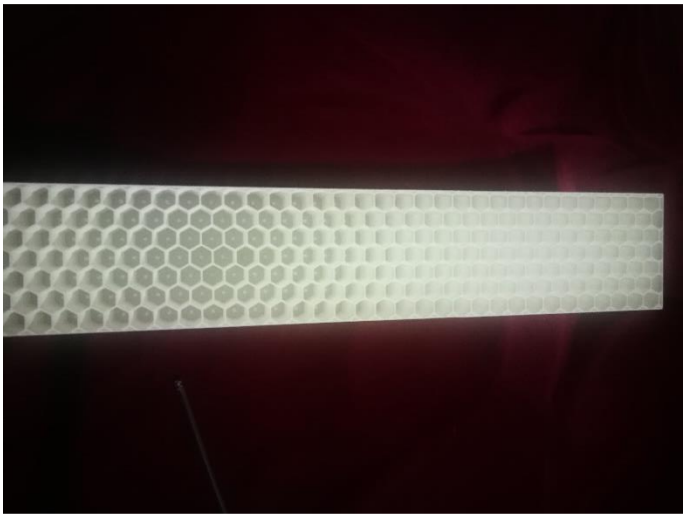

Fig.7 Liner prototype.

4.2. Results

The transmission loss (TL) of the liner for 4 different mean flow speeds is shown in Fig. 8. The TL is obtained by assuming that only plane waves propagate in the downstream duct segment and a mode decomposition technique is used to separate the upstream and downstream propagating waves. Results show that the maximum attenuation occurs around 540Hz for the no flow case which is smaller than that predicted by the proposed model but is larger than that measured in the impedance tube. With the increase of flow speed, the peak gradually increases and the attenuation performance decreases. For the maximum flow speed tested in the current work, the TL is below 4dB in general. The deterioration of the performance may be attributed to the increase of the resistance of the surface impedance which leads to an impedance mistach. Therefore, further effort should be made to accurately characterize the liner impedance for better noise control performance.

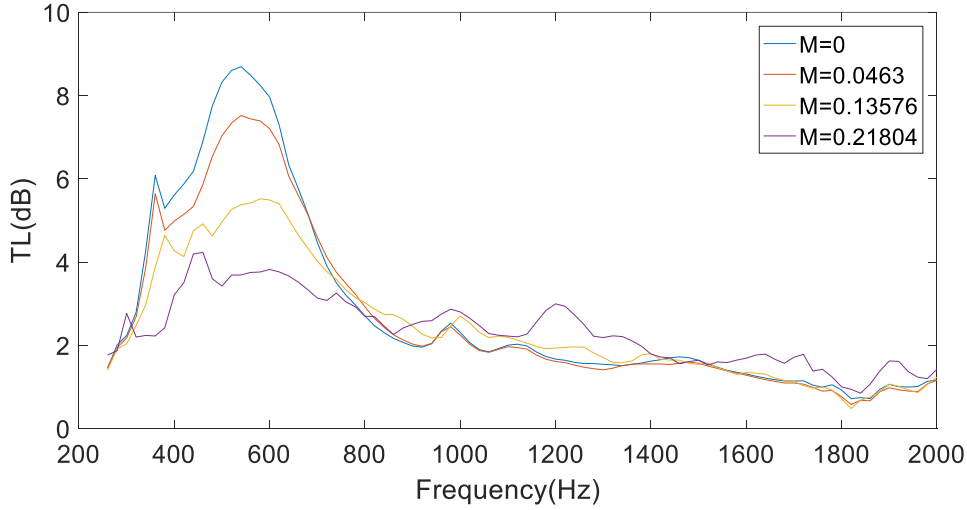

Fig.8 Transmission loss at different flow speeds.

5. CONCLUSIONS

A preliminary study of a thin acoustic liner by integrating extended tube to the microperforated panel is presented. An analytical model is developed to predict the acoustic property of the liner. Although the model is in good agreement with that in the literature and the FEM result, a noticeable discrepancy can be found with the measurement result. For extended tubes with such small radius, the influence of the end correction cannot be neglected, so further efforts should be made in this direction to improve the model.

The proposed model is used to design an acoustic liner for duct noise control. Measurement in a flow duct shows that the attenuation decreases with the flow speed and the frequency where the maximum attenuation occurs increases with the flow speed. Compared with conventional liners, the resonance frequency of the liner is significantly reduced, which makes it a promising noise control technique for future aircraft engine nacelle.

6. ACKNOWEDGEMENTS

This work is partially supported by Shanghai Pujiang Program (18PJ1405600).

7. REFERENCES

1. Allam, S., & Åbom, M. (2011). *A new type of muffler based on microperforated tubes*. Journal of vibration and acoustics, 133(3), 031005.
2. Bravo, T., Maury, C., & Pinhède, C. (2016). *Optimisation of micro-perforated cylindrical silencers in linear and nonlinear regimes*. Journal of Sound and Vibration, 363, 359-379.
3. Tao, J., Jing, R., & Qiu, X. (2014). *Sound absorption of a finite micro-perforated panel backed by a shunted loudspeaker.* The Journal of the Acoustical Society of America, 135(1), 231-238.
4. Chen, C., Du, Z., Hu, G., & Yang, J. (2017). *A low-frequency sound absorbing material with subwavelength thickness*. Applied Physics Letters, 110(22), 221903.
5. Sugimoto, R., Astley, R. J., & Murray, P. B. (2010, August). *Low frequency liners for turbofan engines.* In Proceedings of the 20th International Congress on Acoustics (p. 4).
6. Gai, X. L., Xing, T., Li, X. H., Zhang, B., Cai, Z. N., & Wang, F. (2018). *Sound absorption properties of microperforated panel with membrane cell and mass blocks composite structure.* Applied Acoustics, 137, 98-107.
7. Lu, Y., Li, X., Tian, J., & Wei, W. (2001, August). *The perforated panel resonator with flexible tube bundle and its acoustical measurements.* In INTER-NOISE and NOISE-CON Congress and Conference Proceedings (Vol. 2001, No. 7, pp. 360-363). Institute of Noise Control Engineering.
8. Chang, D., Lu, F., Jin, W., & Liu, B. (2018). *Low-frequency sound absorptive properties of double-layer perforated plate under grazing flow.* Applied Acoustics, 130, 115-123.
9. Huang, S., Fang, X., Wang, X., Assouar, B., Cheng, Q., & Li, Y. (2019). *Acoustic perfect absorbers via Helmholtz resonators with embedded apertures*. The Journal of the Acoustical Society of America, 145(1), 254-262.
10. Yang, C., & Cheng, L. (2016). *Sound absorption of microperforated panels inside compact acoustic enclosures*. Journal of sound and vibration, 360, 140-155.
11. Simon, F. (2018). *Long elastic open neck acoustic resonator for low frequency absorption*. Journal of Sound and Vibration, 421, 1-16.